IET Optoelectronics

Special Issue on Optical-Wireless Communications

IET Journals
The Institution of Engineering and Technology

Semiconductor optical amplifiers in negative-exponential fading: regenerators and pre-amplifiers

ISSN 1751-8768
Received on 15th October 2014
Revised on 16th March 2015
Accepted on 7th April 2015
doi: 10.1049/iet-opt.2014.0123
www.ietdl.org

Nikos C. Sagias, Kostas Yiannopoulos ✉, *Anthony C. Boucouvalas*

Department of Informatics & Telecommunications, University of Peloponnese, Akadimaikou G. K. Vlahou, 22100 Tripoli, Greece
✉ *E-mail: kyianno@uop.gr*

Abstract: In this study, the authors discuss the mitigation of negative-exponential fading in optical wireless communication systems. The mitigation technique involves the utilisation of a semiconductor optical amplifier (SOA) that, depending on the link arrangement, acts either as regenerator or pre-amplifier. As a regenerator, the SOA gain saturates during normal link operation and increases when the link experiences a fade. This unbalanced SOA operation serves towards the equalisation of the signal power at its output and fades become less severe and of reduced duration. The analytical results predict that the fade probability is reduced by over 90% and the scintillation index is improved by 75% for an optimal level of the received power. Moreover, the average duration of fades is also reduced by 68% for the same power level. As a pre-amplifier, the SOA modifies the noise statistics at the receiver and provides a static sensitivity increase of at least 10 dB at 10 Gb/s, depending on the bit-error-rate (BER) target. The analytical results show that this sensitivity improvement imparts a reduction of one order of magnitude on the average BER, of at least 94% on the outage probability and of at least 78% on the average duration of fades.

1 Introduction

The mitigation of fades is an important topic in outdoor optical wireless (OW) systems, where atmospheric turbulence induces time-varying changes to the refractive index, which in turn affect the amplitude, phase and propagation direction of the optical signal [1–3]. These changes ultimately manifest as time-varying power fluctuations of the received signal and when the turbulence is intense enough, the received power decreases below the receiver sensitivity and the link is lost. This corresponds to a fade event, which affects the optical wireless communication (OWC) system both in terms of capacity, as well as latency. Owing to the negative impact of fades on the OWC systems performance, a number of techniques have been proposed for decreasing the fade probability and the average fade duration (AFD), and therefore, for minimising their detrimental effect. In weak (log-normal) fading conditions it is typically sufficient to utilise an aperture-averaging technique, where a large-aperture receiver collects stray light [4, 5] or beam focusing [6]. The mitigation of more intense (gamma–gamma) fading, however, requires spatial or temporal diversity techniques [7–14]. Alternatively, more advance mitigation techniques can be implemented using aperture averaging and diversity in conjunction with relaying [15], amplification [16–18] and/or coding schemes [19–23], which essentially adapt the transmission rate with the channel capacity.

Within the context of fade mitigation, we have previously reported and analysed the utilisation of semiconductor optical amplifiers (SOAs) in outdoor OWC systems in two distinct modes of operation. Both modes, re-generation and pre-amplification, rely on utilising a SOA before opto-electronic conversion in a setup that is illustrated in Fig. 1. Under partial saturation, the SOA can act as a regenerator that mitigates fades by providing unbalanced gain to the incoming OW signal [18]. If the link is in a fade state, then the SOA is not saturated by the received signal and provides linear gain, whereas the received signal saturates the SOA and experiences limited or no gain at all during the absence of fades. The gain saturation effect provides increased amplification to the fade impaired segments of the signal and, as a result, the signal power fluctuations become less intense at the SOA output [18, 24]. On the other hand, if the average received optical power is not sufficient to saturate the SOA, then the device acts as an almost linear amplifier regardless of the channel state. In this mode of operation, a second additional benefit can be obtained from the improvement that is observed at the receiver sensitivity because of the signal and noise beating process on the photo-diode [25, 26]. In [27], we demonstrated that the sensitivity improvement translates directly into a link gain that drastically improves the OWC system performance in terms of the attained bit-error-rate (BER).

Although previous works have demonstrated the potential of SOA-based fade mitigation, the fading conditions that were considered correspond to either weak (log-normal) or moderate (gamma–gamma) turbulence. It is still of interest, however, to investigate the performance of the proposed technique in more adverse (saturated) fading conditions that appear over increased OWC link lengths and/or intense turbulence. In this regime, the received power fluctuations are typically considered to follow a negative-exponential distribution [28–33], which corresponds to the propagation of light beams through a very large number of scattering cells [34]. The primary goal of this work is to demonstrate the applicability of SOA-based regeneration and pre-amplification in this intense fading environment and discuss in a quantitative fashion the performance improvement that can be achieved. To this end, we first derive in Section 2 an analytical model for calculating the first- and second-order statistics of the SOA-based regenerator. We then utilise the presented analytical model to assess restorative properties of the SOA and demonstrate that a significant reduction of over 90 and 68% can be expected for the fade probability and duration, respectively. In addition, we investigate the quality of the signal in terms of the scintillation index (SI) and show that it can also be reduced by 75% at maximum. As far as the SOA pre-amplifier is concerned, we derive in Section 3 a mathematical framework that evaluates the system performance in terms of the BER that is attainable at each channel state. The model takes into account all noise variances that arise from the signal and noise beating process and associates them with the channel state, thus enabling the treatment of the system BER as a random variable whose values are determined by the negative-exponential statistics. We then utilise the presented

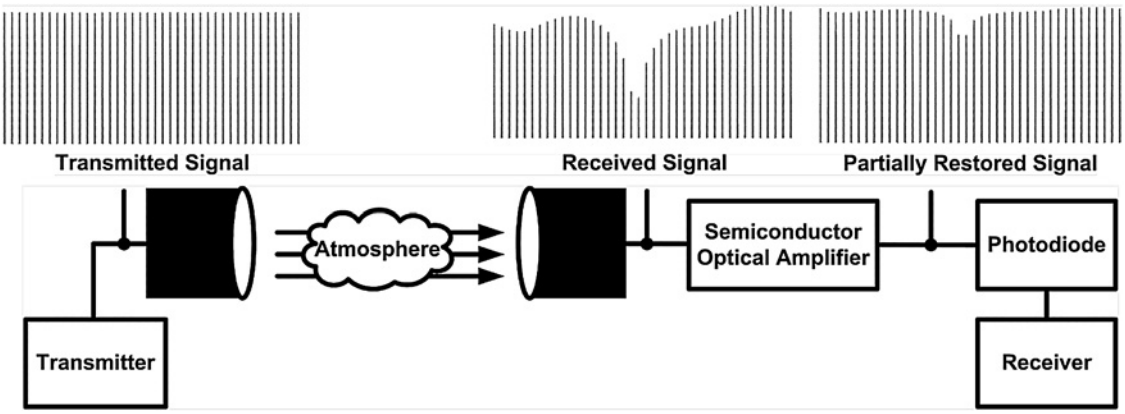

Fig. 1 *Proposed fade mitigation setup and principle of operation*

framework to analytically calculate metrics, such as the average BER, the outage probability and the AFD of the SOA-assisted system. The analytical results demonstrate that the SOA improves the average BER by one order of magnitude, the outage probability by over 94% and the average duration of fades by over 78% for practical receiver arrangements. Finally, we shortly discuss the impact of background noise on the pre-amplifier performance.

2 SOA as regenerator

In the current section, we first analytically calculate the probability density function (pdf) of the signal at the SOA output, which will enable the derivation of the fade probability and the SI. Both are the two most commonly considered first-order metrics that describe the signal quality in the presence of fades. Our goal is to demonstrate that the deployment of the SOA and its unbalanced gain saturation results in a signal that, although not fully restored, is of superior quality when compared with the original negative-exponential impaired one, and as a result the SOA essentially acts as a regenerator. The fade mitigation capabilities of the SOA-based equaliser are also demonstrated by the second-order statistics of the signal at the output of the SOA. Even though the SOA drastically reduces the fade probability, as we will show next, fades are still expected to occur and it is of practical importance to have an estimation of the AFD. The AFD affects the OWC system latency and its evaluation is particularly useful when considering temporal diversity techniques, since it provides an estimate of the required buffering, as well as when designing link layer automatic request protocols in which the frame and window sizes should be tailored so that a full-window transmission exceeds the fade duration.

2.1 SOA output power pdf

We begin our analysis by considering that the average power P_{in} of each received pulse at the SOA input follows the channel response. Under strong fading conditions P_{in} can be modelled as a negative-exponential random variable [34] with a pdf equal to

$$f_{P_{\text{in}}}(z) = \frac{1}{\bar{P}_{\text{in}}} \exp\left(-\frac{z}{\bar{P}_{\text{in}}}\right) \tag{1}$$

where $\bar{P}_{\text{in}}$ is the average received optical power. The received pulses are driven to the SOA and each pulse experiences a gain that is dependent on its energy. We assume that the gain recovery time is limited to less than one bit period T_{b}, so that the SOA fully recovers to its small signal G gain after each incoming pulse. The input U_{in} and output U_{out} pulse energies obey [35, 36]

$$U_{\text{out}} = U_{\text{sat}} \log\left[1 + G\left(\exp\left(\frac{U_{\text{in}}}{U_{\text{sat}}}\right) - 1\right)\right] \tag{2}$$

with U_{sat} being the SOA saturation energy. Input and output pulse energies are proportionally related to average optical powers

$$U_{\text{in}} = P_{\text{in}} T_{\text{b}} \tag{3a}$$

and

$$U_{\text{out}} = P_{\text{out}} T_{\text{b}} \tag{3b}$$

and as a result (2) can be re-written as

$$P_{\text{out}} = P_{\text{sat}} \log\left[1 + G\left(\exp\left(\frac{P_{\text{in}}}{P_{\text{sat}}}\right) - 1\right)\right] \tag{4}$$

where P_{sat} is the rate-dependent saturation parameter of the SOA

$$P_{\text{sat}} = \frac{U_{\text{sat}}}{T_{\text{b}}} \tag{5}$$

The pdf of the optical signal envelope at the output of the SOA is calculated by combining (1) and (4)

$$f_{P_{\text{out}}}(z) = \frac{1}{G\bar{P}_{\text{in}}} \exp\left(\frac{z}{P_{\text{sat}}}\right) \left(\mathcal{T}\left(\frac{z}{P_{\text{sat}}}\right)\right)^{-(P_{\text{sat}}/\bar{P}_{\text{in}})-1} \tag{6}$$

with $\mathcal{T}(x) = [G - 1 + \exp(x)]/G$. For discussion purposes, we further define the normalisation parameters r (normalised input power) and u (normalised output power)

$$r = \frac{\bar{P}_{\text{in}}}{P_{\text{sat}}} \tag{7a}$$

and

$$u = \frac{P_{\text{out}}}{\bar{P}_{\text{in}}} \tag{7b}$$

to obtain the normalised SOA output power pdf as

$$f_u(z) = \frac{1}{G} \exp(rz) \left(\mathcal{T}(rz)\right)^{-(1/r)-1} \tag{8}$$

IET Optoelectron., 2015, Vol. 9, Iss. 5, pp. 249–256

2.2 First-order statistics

A fade occurs whenever the output power u remains below a predetermined threshold u_τ, and by integrating (8), we find that the fade probability equals to

$$P_{\text{out}} = \Pr\{u < u_\tau\} = \int_0^{u_\tau} f_u(z)\,\mathrm{d}z = 1 - \left(\mathcal{T}\left(ru_\tau\right)\right)^{-1/r} \tag{9}$$

The fade probability is plotted in Fig. 2 against the normalised receiver power threshold ρ

$$\rho = \frac{u_\tau}{u_{\text{rms}}} \tag{10}$$

where u_{rms} is numerically evaluated using

$$u_{\text{rms}}^2 = \frac{1}{G}\int_0^{\infty} z^2 \exp(rz)\left(\mathcal{T}(rz)\right)^{-(1/r)-1}\,\mathrm{d}z \tag{11}$$

This normalisation is performed so as to take into account the average static gain which is provided by the SOA, and thus, compare pdfs that correspond to different average output powers in a fair manner.

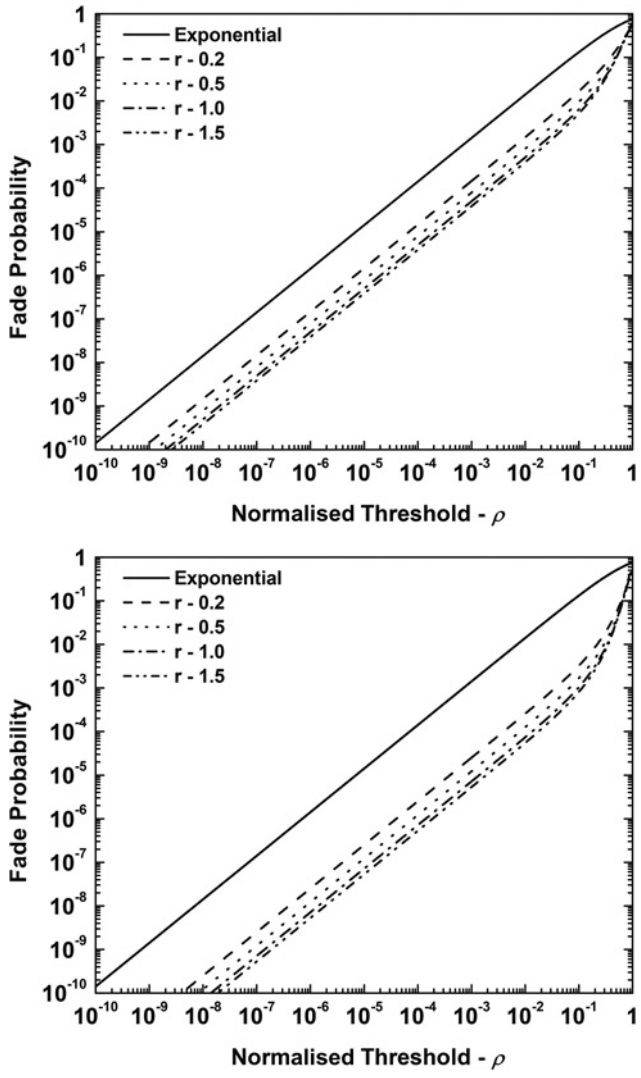

Fig. 2 *Fade probability at the output of the SOA against the normalised threshold ρ*

SOA small signal gain G equals 20 dB (top) and 30 dB (bottom)

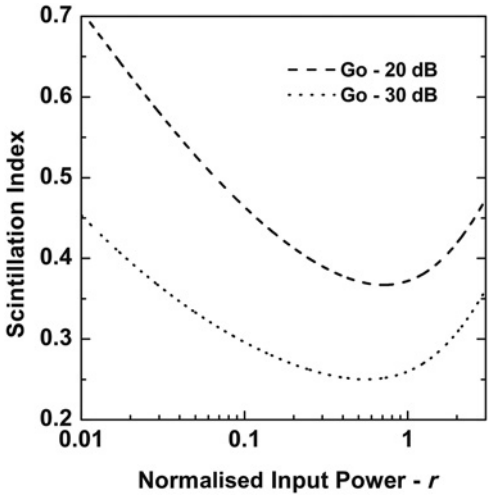

Fig. 3 *SI the output of the SOA against the normalised input power r*

Fig. 2 shows that the fade probability is considerably decreased when the SOA is deployed in comparison with the incoming negative-exponential signal. A fade probability decrease of over 90% is predicted for a 20 dB small-signal gain SOA, whereas a 30 dB gain device further reduces the fade probability by 95%. This is expected from the SOA response as detailed in (2), since higher gain devices lead to better equalisation of the output pulse energies. The results also suggest that increasing the average input power r is always beneficial, still the attained benefit saturates and input powers of over 1 do not yield a significant restorative improvement. This last observation can be further explored by numerically evaluating the SI of the signal at the SOA output

$$\sigma_u = \frac{\sqrt{u_{\text{rms}}^2 - \bar{u}^2}}{\bar{u}} \tag{12}$$

where

$$\bar{u} = \frac{1}{G}\int_0^{\infty} z \exp(rz)\left(\mathcal{T}(rz)\right)^{-(1/r)-1}\,\mathrm{d}z \tag{13}$$

The SI is plotted in Fig. 3 against the normalised input power r for SOAs with 20 and 30 dB small-signal gains. The figure shows that the output signal SI values are significantly lower than those of the original negative-exponential (SI =1), which serves to verify the beneficial impact of the equalisation process. Similar to the fade probability results, high gain SOAs are also capable of attaining lower SIs as compared to lower gain ones and are therefore preferable. Finally, it is noteworthy to mention that the SI is minimised for input powers approximately equal to the saturation parameter P_{sat} of the SOA. This is expected from the SOA operation, since low average input powers lead to a non-saturated device that always provides linear gain, thus no equalisation, to both fade impaired and non-impaired pulses. In the totally opposite regime, a fully saturated device will provide unity gain to all pulses irrespective of their energy and as a result fades are not equalised, as well. The optimal point of operation corresponds to a partially saturated SOA ($r \simeq 1.0$) that provides increasing gain to weaker pulses and thus restores the input signal to some extent.

2.3 Second-order statistics

The AFD at the output of the SOA is calculated from the output signal level crossing rate (LCR), which in turn requires the knowledge of the joint pdf between the output signal and its time derivative. The joint pdf at the SOA output is calculated from the

joint pdf of the exponentially faded input signal, given by [37]

$$f_{v,\dot{v}}(z,\, w) = f_v(z)\frac{1}{\sqrt{4\pi z\bar{P}_{\text{in}}r(0)}}\exp\left(-\frac{w^2}{4z\bar{P}_{\text{in}}r(0)}\right) \tag{14}$$

where

$$f_v(z) = \exp(-z) \tag{15}$$

$r(\tau)$ is the normalised covariance function that describes the rapidity of fading and the dot operator corresponds to the time derivative. To calculate the joint pdf at the SOA output we utilise (4) to obtain the relations between the input v and output u signal powers and their derivatives, resulting in

$$v = \frac{1}{r}\log\left[\frac{G-1+\exp(ru)}{G}\right] \tag{16a}$$

$$\dot{v} = \frac{\exp(ru)}{G-1+\exp(ru)}\dot{u} \tag{16b}$$

After applying the variable transform of (16) into (14), we find that

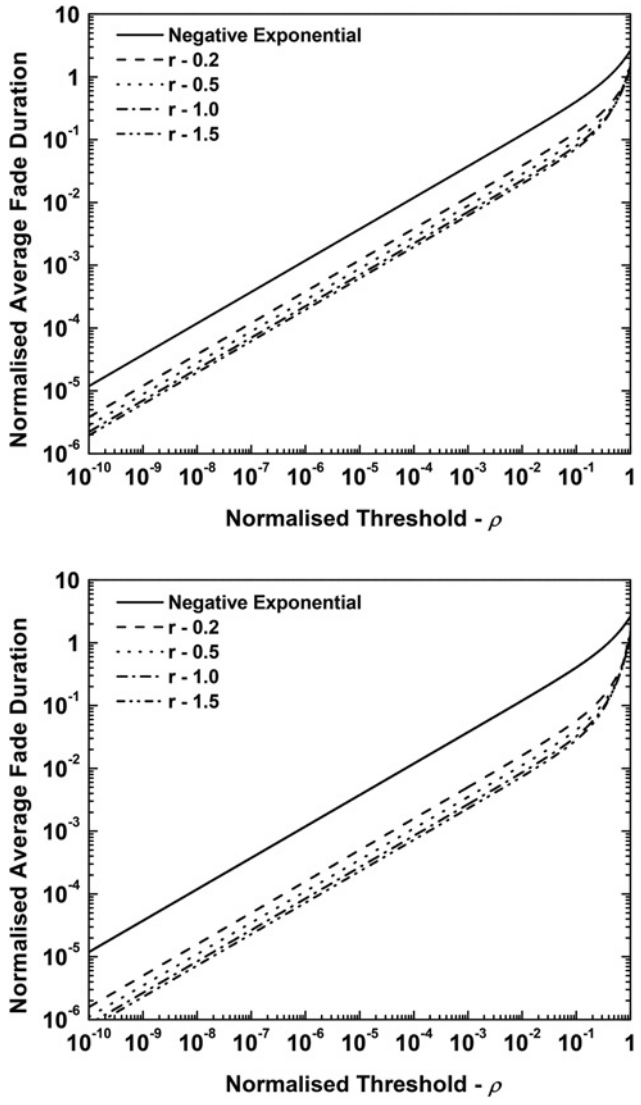

Fig. 4 *Average fade duration at the output of the SOA against the normalised threshold ρ*

SOA small signal gain G equals 20 dB (top) and 30 dB (bottom)

the joint pdf at the SOA equals

$$f_{u,\dot{u}}(z,\, w) = f_u(z)\frac{\exp\left(-w^2/2\sigma^2_{\text{SOA}}\right)}{\sqrt{2\pi}\sigma_{\text{SOA}}} \tag{17}$$

with variance σ_{SOA} being defined as

$$\sigma^2_{\text{SOA}} = \frac{2P_{\text{sat}}\bar{P}_{\text{in}}r(0)\left(G-1+\exp\left(z/P_{\text{sat}}\right)\right)^2\log\left[\mathcal{T}\left(z/P_{\text{sat}}\right)\right]}{\exp\left(2z/P_{\text{sat}}\right)} \tag{18}$$

By integrating (17) with respect to the time derivative w and keeping the normalisation definitions of (7), we calculate the LCR at the output of the SOA

$$\begin{aligned}\text{LCR}\left(u_\tau\right) &= \int_0^\infty f_{u,\dot{u}}(u_\tau,\, w)w\,\text{d}w \\ &= \sqrt{\frac{r(0)}{\pi}}\left(\frac{1}{r}\log\left[\mathcal{T}\left(ru_\tau\right)\right]\right)^{1/2}\left(\mathcal{T}\left(ru_\tau\right)\right)^{-1/r}\end{aligned} \tag{19}$$

and the AFD is finally derived after combining the fade probability and the LCR as

$$\text{AFD}\left(u_\tau\right) = \sqrt{\frac{\pi}{r(0)}}\frac{\left(\mathcal{T}\left(ru_\tau\right)\right)^{1/r}-1}{\left((1/r)\log\left[\mathcal{T}\left(ru_\tau\right)\right]\right)^{1/2}} \tag{20}$$

Equation (20) is plotted in Fig. 4 against the normalised threshold ρ. The figure suggests that the 20 dB-gain SOA reduces the duration of fades by 68–84%, whereas the 30 dB-gain SOA achieves an even better reduction of 87–94%. As a result the duration of fades, and therefore the system latency, can be decreased by up to two orders of magnitude by utilising the SOA-based SOA, provided that the SOA is saturated to the appropriate level. Similar to the first-order statistics, a signal power approximately equal to the saturation parameter is adequate to attain maximum AFD reduction.

3 SOA as pre-amplifier

In this section, we first derive the mathematical model that will enable the BER assessment the pre-amplified OWC system. To this end, we briefly detail the signal and noise properties of the SOA output and then correlate the system BER with the OWC channel state. We further discuss the performance improvement that is introduced by the SOA in the first-order statistics of the OWC system, and in particular the average BER and the outage probability, which provide a measure of the OW link reliability. Apart from these metrics, it is equally important to evaluate the second-order statistics of the pre-amplified system. Therefore, similarly to the regenerator analysis, we focus on the analysis for the AFD that is defined as the average duration that the OWC system remains below a desired BER level after a fade event.

3.1 Noise model and BER calculation

We first consider that the SOA generates an optical noise component because of the amplified spontaneous emission (ASE), which is described by the ASE spectral density

$$P_{\text{n}} = n_{\text{sp}}h\frac{c}{\lambda} \tag{21}$$

where c is the vacuum light speed, h is the Planck constant, n_{sp} is the population inversion factor and λ denotes the wavelength. The optical signal and the ASE beat on the square-law detector of the receiver (photodiode) and as a result several electrical noise components appear at the photodiode output. The associated noise variances are denoted as thermal, shot, signal-spontaneous beating

Table 1 System parameters

Parameter	Symbol	Value
wavelength	λ	1550 nm
line rate	T_b^{-1}	10 Gb/s
SOA small-signal gain	G	20 or 30 dB
saturation parameter	P_{sat}	1 mW
population inversion factor	n_{sp}	4.0
photodiode responsivity	R	1.25 A/W
receiver temperature	T	300K
resistor load	R_L	100 Ω
electrical noise figure	F_n	3 dB
electrical bandwidth	B_e	7 GHz
optical bandwidth	B_o	50 GHz

and spontaneous-spontaneous beating, and are calculated as

$$\sigma_{th}^2 = \frac{4k_B T F_n B_e}{R_L} \tag{22a}$$

$$\sigma_{shot}^2(z) = 2qR\big(P_{out}(z) + (G-1)P_n B_o\big)B_e \tag{22b}$$

$$\sigma_{sig-sp}^2(z) = 4R^2 P_{out}(z)(G-1)P_n B_e \tag{22c}$$

and

$$\sigma_{sp-sp}^2 = R^2\big((G-1)P_n\big)^2(2B_o - B_e)B_e \tag{22d}$$

respectively. In (22), B_e and B_o are the electrical and optical bandwidths, respectively, R is the photodiode responsivity, T is the receiver temperature, k_B denotes the Boltzmann constant, F_n is the electric noise figure and R_L is the resistor load. All respective parameters and the values that are used for the presentation are summarised in Table 1.

Given (4) and (22), the signal and noise powers in the '1' and '0' symbols are directly calculated as

$$I_1(z) = RP_{out}(z) \tag{23a}$$

$$\sigma_1^2(z) = \sigma_{th}^2 + \sigma_{shot}^2(z) + \sigma_{sig-sp}^2(z) + \sigma_{sp-sp}^2 \tag{23b}$$

and

$$I_0 = 0 \tag{24a}$$

$$\sigma_0^2 = \sigma_{th}^2 + \sigma_{shot}^2(0) + \sigma_{sp-sp}^2 \tag{24b}$$

respectively. Following the above, the BER performance of the system is evaluated by

$$\mathrm{BER}(z) = \frac{1}{2}\mathrm{erfc}\left(\frac{Q(z)}{\sqrt{2}}\right) \tag{25}$$

with

$$Q(z) = \frac{I_1(z)}{\sigma_0 + \sigma_1(z)} \tag{26}$$

In (25), it is assumed that the receiver is capable of estimating the Channel State Information (CSI-capable) and setting its decision threshold on a symbol-by-symbol fashion to [38]

$$I_{th}(z) = \frac{\sigma_0 I_1(z)}{\sigma_0 + \sigma_1(z)} \tag{27}$$

3.2 First-order statistics

The average BER is calculated after integrating the BER variable over all possible negative-exponential channel states following

$$\overline{\mathrm{BER}} = \frac{1}{2}\int_0^\infty \mathrm{erfc}\left(\frac{Q(z)}{\sqrt{2}}\right) f_{P_{in}}(z)\,dz \tag{28}$$

The integral is evaluated in a numerical fashion from the values of Table 1 and the results are plotted in Fig. 5 for two SOAs with 20 and 30 dB small signal gains. The figure clearly demonstrates a very significant improvement of the average BER of the system with the SOA and a 16 dB gain in the link budget is observed at any fixed BER level. This is expected from the sensitivity increase that is brought about by the SOA, which equals 14.3 dB at a BER of 10^{-3} and 12.5–13.8 dB at a BER of 10^{-6} given the numerical values under consideration. Moreover, the deployment of the SOA improves the average BER at least one order of magnitude for the presented input powers, thus the SOA adds to the reliability of the system and can contribute towards lowering the fade margin that is required in a practical system.

The exact contribution of the SOA to the link margin, however, can only be explored via the outage probability, since real-world systems are designed with a specific maximum acceptable BER level in mind, and additional techniques (mainly forward error correction) are introduced to recover from link errors. In these systems, an outage occurs whenever the BER at the receiver remains below the pre-defined target level BER_0, and following the analysis presented in the previous section the outage probability is calculated by

$$P_{out} = \Pr\{\mathrm{BER}(z) > \mathrm{BER}_0\} \tag{29}$$

or equivalently by

$$P_{out} = \Pr\{z \le P_s\} = \int_0^{P_s} f_{P_{in}}(z)\,dz = 1 - \exp\left(-\frac{P_s}{\overline{P}_{in}}\right) \tag{30}$$

where P_s is the receiver sensitivity that is required to achieve BER_0. The equivalence of (29) and (30) is justified from the fact that BER_0 is exceeded whenever the input power remains below the corresponding sensitivity P_s. Furthermore, the corresponding receiver sensitivity is obtained after numerically solving

$$\mathrm{BER}(P_s) = \frac{1}{2}\mathrm{erfc}\left(\frac{Q(P_s)}{\sqrt{2}}\right) = \mathrm{BER}_0 \tag{31}$$

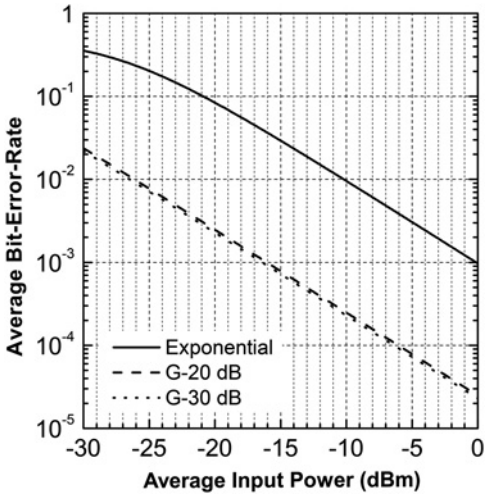

Fig. 5 *Average BER against the average input power*

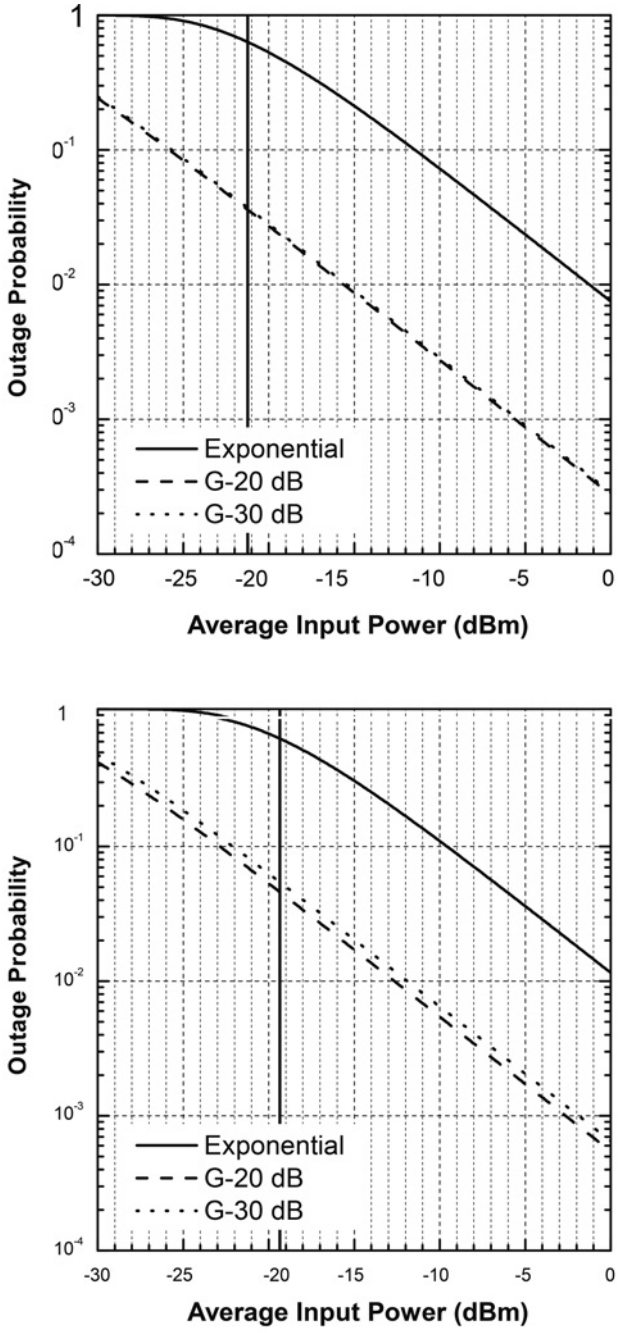

Fig. 6 *Outage probability against the average input power for $BER_0 = 10^{-3}$ (top) and $BER_0 = 10^{-6}$ (bottom)*

Solid vertical line corresponds to the receiver sensitivity without the SOA

The outage probability is plotted in Fig. 6, which illustrates the performance of a SOA-assisted receiver assuming acceptable BER levels of 10^{-3} and 10^{-6}. In agreement with the average BER results, the figure shows that a significant gain in the link budget is obtained by using the SOA, still the gain is a couple of dBs lower than this predicted by the average BER analysis. In fact, the link budget gain is exactly equal to the receiver sensitivity improvement that the SOA introduces and equals 14.3 dB for a maximum BER of 10^{-3} and 12.5–13.8 dB for a maximum BER of 10^{-6}, depending on the SOA small signal gain. With respect to the outage probability itself, the SOA-assisted system exhibits a reduced outage probability for all practically anticipated power levels. The reduction amounts to 96% for the 10^{-3} and over 94% for the 10^{-6} BER level, and exceeds the 90% reduction that is required to increase the system percentile availability by one additional '9'.

3.3 Second-order statistics

The AFD is calculated from the outage probability (29) and the LCR of the OWC link. For negative-exponential fading the LCR (normalised over the maximum Doppler frequency shift) is given by

$$\mathrm{LCR}(P_\mathrm{s}) = \exp\left(-\frac{P_\mathrm{s}}{\bar{P}_\mathrm{in}}\right)\sqrt{\left(\frac{P_\mathrm{s}}{\bar{P}_\mathrm{in}}\right)} \tag{32}$$

As we detail in [27], it is sufficient for the pre-amplified system to evaluate the LCR at the receiver sensitivity P_s that is the required to attain the desired BER level BER_0 following (31). This results simplifies the calculation of the AFD, which is obtained in a straight-forward manner as

$$\mathrm{AFD}(P_\mathrm{s}) = \frac{\Pr\{z \le P_\mathrm{s}\}}{\mathrm{LCR}(P_\mathrm{s})} = \frac{\exp(P_\mathrm{s}/\bar{P}_\mathrm{in}) - 1}{\sqrt{(P_\mathrm{s}/\bar{P}_\mathrm{in})}} \tag{33}$$

Equation (33) is plotted in Fig. 7 for a system with maximum BER level of 10^{-3} and 10^{-6}. It can be verified from the figure that the SOA has a significant impact on the OW system AFD, owing to the expected sensitivity improvement. As a result, the link margin of 14.3 dB for the BER of 10^{-3} and 12.5–13.8 dB for the BER of 10^{-6} that was calculated in the outage probability analysis is also valid for the AFD analysis. With respect to the AFD itself, an AFD improvement of over 80% is predicted for the 10^{-3} BER level, whereas the corresponding improvement is marginally reduced to 78% for the 10^{-6} BER level.

Following the above, the SOA is well capable of drastically reducing both the probability of a fade and its average duration thus enabling a more reliable and lower latency outdoor OW system. In addition, the same link margin that is predicted for the outage probability in the first-order statistics analysis is also observed for the AFD and as a result the SOA-assisted receiver performance can be thoroughly described in a systematic fashion by the required sensitivity improvement and the statistics that govern fading.

3.4 Impact of the background noise

A final aspect that is interesting to address with respect to the pre-amplifier mode relates to the impact of the background noise. Despite the fact that, the background noise is generally lower in the 1550 nm window as compared with the 850 nm one, since the solar radiation reduces at increasing wavelengths, any background noise that is coupled to the SOA receives a significant level of amplification. As a result, both the spontaneous and background noises will manifest at the SOA output and a degradation of the system performance is expected. For the purposes of this work, we assume that background radiation has a uniform spectral density P_bg within the optical bandwidth B_o of the receiver. The background radiation is independent from the ASE noise generated in the SOA [39], and it is straightforward to modify the noise variances in (22) as

$$\sigma^2_{\mathrm{shot}}(z) = 2qR\Big(P_{\mathrm{out}}(z) + \Big((G-1)P_\mathrm{n} + GP_\mathrm{bg}\Big)B_\mathrm{o}\Big)B_\mathrm{e} \tag{34a}$$

$$\sigma^2_{\mathrm{sig-sp,bg}}(z) = 4R^2P_{\mathrm{out}}(z)\Big((G-1)P_\mathrm{n} + GP_\mathrm{bg}\Big)B_\mathrm{e} \tag{34b}$$

and

$$\sigma^2_{\mathrm{sp,bg-sp,bg}} = R^2\Big((G-1)P_\mathrm{n} + GP_\mathrm{bg}\Big)^2(2B_\mathrm{o} - B_\mathrm{e})B_\mathrm{e} \tag{34c}$$

Again, a worst-case scenario is considered for the system operation in (34), where the background radiation does not saturate the SOA gain and receives small-signal gain amplification.

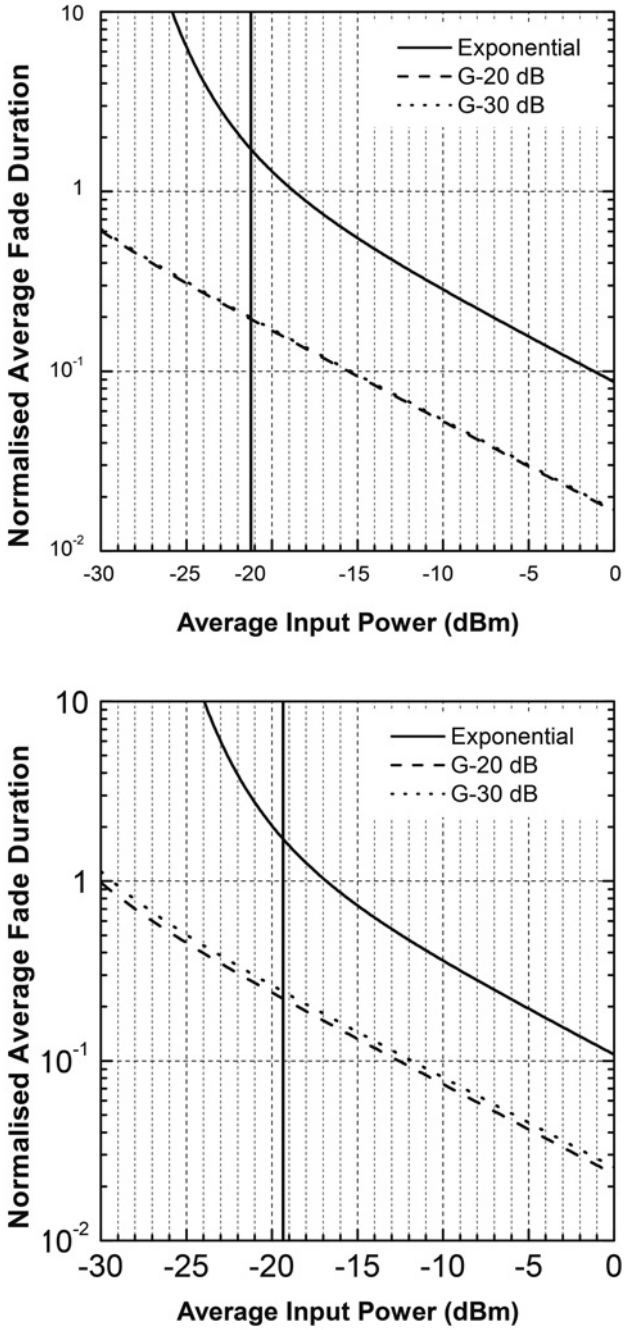

Fig. 7 *Average fade duration against the average input power for* $BER_0 = 10^{-3}$ *(top) and* $BER_0 = 10^{-6}$ *(bottom)*

Solid vertical line corresponds to the receiver sensitivity without the SOA

The exact power level of P_{bg} is calculated by parameters that include the environmental conditions and the field of view of the receiver, following a more detailed analysis that can be found elsewhere [40]. It is not the absolute value of P_{bg}, however, that plays an important role in the pre-amplifier operation; rather it is the relative magnitude of P_{bg} with respect to P_n that proves critical, since both noise powers receive approximately the same gain G. This is presented in Fig. 8, which plots the average BER performance of the SOA-assisted system for the cases of (a) zero level background noise, (b) equal powers of background and ASE noise and (c) background noise power ten times stronger than the ASE. As the figure suggests, the inclusion of the background radiation introduces a power penalty that is proportional to the imparted noise increase, and amounts to 3 dB and (slightly over) 10 dB, respectively, when a 20 dB gain SOA is deployed. This

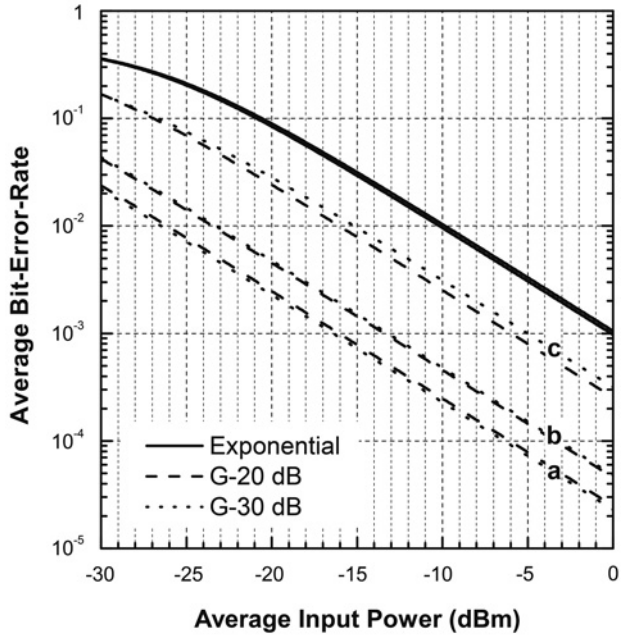

Fig. 8 *Average BER against the average input power for*

a Zero level background noise
b Equal powers of background and ASE noise
c Background noise power ten times stronger than the ASE

can be justified theoretically, since the signal-noise beating term is the dominant electrical noise component and the Q-factor can be approximated as

$$Q = \frac{I_1}{\sigma_0 + \sigma_1} \simeq \frac{I_1}{\sigma_1} \simeq \frac{I_1}{\sigma_{\text{sig-sp,bg}}} \propto \sqrt{\frac{P_{\text{out}}}{(G-1)P_n + GP_{bg}}} \tag{35}$$

Consequently, the introduced power penalty is approximately equal to the increase in the optical noise. As far as the 30 dB gain SOA is concerned, the power penalty is higher since both the signal-noise and noise-noise beating terms must be taken into account, especially when the background radiation dominates over the ASE. In contrast, the original non-amplified OWC system presents a totally different behaviour and a very limited power penalty, less than 0.5 dB, is observed when background noise is present. This is also theoretically expected, since the thermal noise dominates the receiver and the Q-factor is relatively insensitive to the noise components that correspond to the background radiation. Following the above, the deployment of the pre-amplifier is only beneficial when the background noise can be kept lower than or comparable with the ASE.

4 Conclusions

We have evaluated in an analytical fashion the performance of a SOA-assisted outdoor OWC link in the negative-exponential fading regime. To this end, we provided a mathematical framework that fully describes the SOA operation both as a regenerator and pre-amplifier and derived analytical results for key first- and second-order statistics of the system, including the SI, outage probability, average BER and fade duration. The presented analytical results clearly demonstrate that all the metrics under consideration are improved by a sizable percentage and, consequently, both modes of operation are applicable, although different saturation levels are optimising the SOA performance in each mode.

5 Acknowledgments

This work was funded by the University of Peloponnese internal project FAMOOSE and supported by COST Action IC1101 'Optical Wireless Communications – An Emerging Technology'.

6 References

1 Lawrence, R.S., Strohbehn, J.W.: 'A survey of clear-air propagation effects relevant to optical communications', *Proc. IEEE*, 1970, **58**, (10), pp. 1523–1545
2 Andrews, L.C., Phillips, R.L.: 'Laser beam propagation through random media' (SPIE Press, Bellingham, Washington, 2005, 2nd edn.)
3 Chan, V.W.S.: 'Free-space optical communications', *J. Lightwave. Technol.*, 2006, **24**, (12), pp. 4750–4762
4 Yuksel, H., Milner, S., Davis, C.C.: 'Aperture averaging for optimizing receiver design and system performance on free-space optical communication links', *OSA J. Opt. Netw.*, 2005, **4**, (8), pp. 462–475
5 Vetelino, F.S., Young, C., Andrews, L., Recolons, J.: 'Aperture averaging effects on the probability density of irradiance fluctuations in moderate-to-strong turbulence', *Appl. Opt.*, 2007, **46**, (11), pp. 2099–2108
6 Hulea, M., Ghassemlooy, Z., Rajbhandari, S., Tang, X.: 'Compensating for optical beam scattering and wandering in FSO communications', *J. Lightwave. Technol.*, 2014, **32**, (7), pp. 1323–1328
7 Wilson, S.G., Brandt-Pearce, M., Cao, Q., Baedke, M.: 'Optical repetition MIMO transmission with multi-pulse PPM', *IEEE J. Sel. Areas Commun.*, 2005, **23**, (9), pp. 1901–1910
8 Navidpour, S.M., Uysal, M., Kavehrad, M.: 'BER performance of free-space optical transmission with spatial diversity', *IEEE Trans. Wirel. Commun.*, 2007, **6**, (8), pp. 2813–2819
9 Goldsmith, A., Jafar, S.A., Jindal, N., Vishwanath, S.: 'Capacity limits of MIMO channels', *IEEE J. Sel. Areas Commun.*, 2003, **21**, (5), pp. 684–702
10 Khalighi, M.-A., Schwartz, N., Aitamer, N., Bourennane, S.: 'Fading reduction by aperture averaging and spatial diversity in optical wireless systems', *J. Opt. Commun. Netw.*, 2009, **1**, (6), pp. 580–593
11 García-Zambrana, A., Castillo-Vázquez, C., Castillo-Vázquez, B.: 'Outage performance of MIMO FSO links over strong turbulence and misalignment fading channels', *Opt. Express*, 2011, **19**, (14), pp. 13 480–13 496
12 Trisno, S., Smolyaninov, I.I., Milner, S.D., Davis, C.C.: 'Delayed diversity for fade resistance in optical wireless communication system through simulated turbulence'. Proc. SPIE Optical Transmission Systems and Equipment for WDM Networking III, Philadelphia, PA, October 2004, vol. 5596, pp. 385–394
13 Greco, J.A.: 'Design of the high-speed framing, FEC, and interleaving hardware used in a 5.4 km free-space optical communication experiment'. Proc. SPIE Free-Space Laser Communications IX, San Diego, CA, 2009, vol. 7464
14 Popoola, W.O., Ghassemlooy, Z.: 'BPSK subcarrier intensity modulated free-space optical communications in atmospheric turbulence', *J. Lightwave Technol.*, 2009, **27**, (8), pp. 967–973
15 Datsikas, C.K., Peppas, K.P., Sagias, N.C., Tombras, G.S.: 'Serial free-space optical relaying communications over gamma-gamma atmospheric turbulence channels', *IEEE/OSA J. Opt. Commun. Netw.*, 2010, **2**, (8), pp. 576–586
16 Abtahi, M., Lemieux, P., Mathlouthi, W., Rusch, L.A.: 'Suppression of turbulence-induced scintillation in free-space optical communication systems using saturated optical amplifiers', *J. Lightwave Technol.*, 2006, **24**, (12), pp. 4966–4973
17 Razavi, M., Shapiro, J.H.: 'Wireless optical communications via diversity reception and optical preamplification', *IEEE Trans. Wirel. Commun.*, 2005, **4**, (3), pp. 975–983
18 Yiannopoulos, K., Sagias, N.C., Boucouvalas, A.C.: 'Fade mitigation based on semiconductor optical amplifiers', *J. Lightwave Technol.*, 2013, **31**, (23), pp. 3621–3630
19 Zhu, X., Kahn, J.M.: 'Performance bounds for coded free-space optical communications through atmospheric turbulence channels', *IEEE Trans. Commun.*, 2003, **51**, (8), pp. 1233–1239
20 Djordjevic, I.B.: 'LDPC-coded MIMO optical communication over the atmospheric turbulence channel using q-ary pulse-position modulation', *Opt. Express*, 2007, **15**, (16), pp. 10 026–10 032
21 Henniger, H., David, F., Giggenbach, D., Rapp, C.: 'Evaluation of FEC for the atmospheric optical IM/DD channel'. Proc. SPIE Free-Space Laser Communication Technologies XV, San Jose, CA, 2003, vol. 4975
22 Anguita, A., Neifeld, M.A., Hildner, B., Vasic, B.: 'Rateless coding on experimental temporally correlated FSO channels', *J. Lightwave Technol.*, 2010, **28**, (7), pp. 990–1002
23 Uysal, M., Li, J., Yu, M.: 'Error rate performance analysis of coded free-space optical links over gamma-gamma atmospheric turbulence channels', *IEEE Trans. Wirel. Commun.*, 2006, **5**, (6), pp. 1229–1233
24 Boucouvalas, A.C., Sagias, N.C., Yiannopoulos, K.: 'First order statistics of semiconductor optical amplifier assisted optical wireless systems under log-normal fading'. Proc. Second Int. Workshop on Optical Wireless Communications (IWOW), October 2013, pp. 142–146
25 Olsson, N.A.: 'Lightwave systems with optical amplifiers', *J. Lightwave Technol.*, 1989, **7**, (7), pp. 1071–1082
26 Humblet, P.A., Azizoglu, M.: 'On the bit error rate of lightwave systems with optical amplifiers', *J. Lightwave Technol.*, 1991, **9**, (11), pp. 1576–1582
27 Yiannopoulos, K., Sagias, N.C., Boucouvalas, A.C.: 'On the bit-error-rate performance of semiconductor optical amplifier assisted outdoor optical wireless links', *IEEE J. Sel. Areas Commun.*, 2015, to appear
28 Song, X., Cheng, J.: 'Subcarrier intensity modulated optical wireless communications using noncoherent and differentially coherent modulations', *J. Lightwave Technol.*, 2013, **31**, (12), pp. 1906–1913
29 Hassan, M., Song, X., Cheng, J.: 'Subcarrier intensity modulated wireless optical communications with rectangular qam', *IEEE/OSA J. Opt. Commun. Netw.*, 2012, **4**, (6), pp. 522–532
30 Niu, M., Cheng, J., Holzman, J.F.: 'MIMO architecture for coherent optical wireless communication: system design and performance', *IEEE/OSA J. Opt. Commun. Netw.*, 2013, **5**, (5), pp. 411–420
31 Popoola, W.O., Ghassemlooy, Z., Ahmadi, V.: 'Performance of sub-carrier modulated fre-space optical communication link in negative exponential atmospheric turbulence environment', *Int. J. Auton. Adapt. Commun. Syst.*, 2008, **1**, (3), pp. 342–355
32 Uysal, M., Li, J.: 'Error performance analysis of coded wireless optical links over atmospheric turbulence channels'. Proc. IEEE Wireless Communications and Networking Conf. (WCNC), March 2004, vol. 4, pp. 2405–2410
33 Garcí a-Zambrana, A., Castillo-Vázquez, B., Castillo-Vázquez, C.: 'Average capacity of fso links with transmit laser selection using non-uniform ook signaling over exponential atmospheric turbulence channels', *Opt. Express*, 2010, **18**, (19), pp. 20 445–20 454
34 Miller, P.F.: 'The probability distribution of a wave at a very large depth within an extended random medium', *J. Phys. A, Math. Gen.*, 1978, **11**, (2), p. 403
35 Agrawal, G.P., Olsson, N.A.: 'Self-phase modulation and spectral broadening of optical pulses in semiconductor laser amplifiers', *IEEE J. Quantum Electron.*, 1989, **25**, (1), pp. 2297–2306
36 Eiselt, M., Pieper, W., Weber, H.G.: 'SLALOM: Semiconductor laser amplifier in a loop mirror', *J. Lightwave Technol.*, 1995, **19**, (10), pp. 2099–2112
37 Primak, S., Kontorovich, V.: 'On the second order statistics of generalized gamma process', *IEEE Trans. Commun.*, 2009, **57**, (4), pp. 910–914
38 Agrawal, G.P.: 'Fiber-optic communication systems', ser. Wiley Series in Microwave and Optical Engineering. (Wiley, 2012)
39 Bayaki, E., Michalopoulos, a.R.S.D.S.: 'EDFA-based all-optical relaying in free-space optical systems', *IEEE Trans. Commun.*, 2012, **60**, (12), pp. 3797–3807
40 Kopeika, N., Bordogna, J.: 'Background noise in optical communication systems', *Proc. IEEE*, 1970, **58**, (10), pp. 1571–1577